

# The Finite Cell Method for Linear Thermoelasticity

N. Zander<sup>a</sup>, S. Kollmannsberger<sup>a</sup>, M. Ruess<sup>a</sup>, Z. Yosibash<sup>b</sup>, E. Rank<sup>a</sup>

<sup>a</sup>*Chair for Computation in Engineering,  
Technische Universität München, Arcisstr. 21, 80333 München, Germany  
{zander,kollmannsberger,ruess,rank}@bv.tum.de*

<sup>b</sup>*Department of Mechanical Engineering,  
Ben-Gurion University, Beer-Sheva 84105, Israel  
zohary@bgu.ac.il*

---

## Abstract

The recently introduced Finite Cell Method (FCM) combines the fictitious domain idea with the benefits of high-order Finite Elements. While previous publications concentrated on single-field applications, this paper demonstrates that the advantages of the method carry over to the multi-physical context of linear thermoelasticity. The ability of the method to converge with exponential rates is illustrated in detail with a benchmark problem. A second example shows that the Finite Cell Method correctly captures the thermoelastic state of a complex problem from engineering practice. Both examples additionally verify that, also for two-field problems, Dirichlet boundary conditions can be weakly imposed on non-conforming meshes by the proposed extension of Nitsche's Method.

*Keywords:* Finite Cell Method (FCM), Fictitious Domain Methods, linear thermoelasticity, multi-physical problems, weak boundary conditions, Nitsche's Method

---

## 1. Introduction

Since the early years of computational engineering, the Finite Element Method has been established as the state-of-the-art approach to solve boundary value problems numerically. Over time, major enhancements to the method allowed for more sophisticated simulations. What remained unchanged was the idea to geometrically resolve the physical domain by the Finite Element mesh. This method's intrinsic need for a conform discretization is a limiting factor in today's engineering practice.

New numerical concepts drop the idea of conforming meshes to circumvent this drawback. Prominent examples are Fictitious and Embedding Domain Methods as well as Immersed Boundary Methods [39, 21, 19, 22, 27]. Also Element-Free Methods [4] and certain variants of the Extended Finite Element Method together with Level Set approaches are part of this category [16, 18, 17, 23]. A comprehensive survey of the different strategies is given in [23]. The common idea of these methods is to reduce the complexity of the mesh generation process by embedding the physical domain  $\Omega_{phy}$  in a fictitious domain  $\Omega_{fict}$  such that their union  $\Omega_{\cup}$  yields a simple geometry.

This strategy is followed by the Finite Cell Method (FCM) introduced in [26] and [11]. In contrast to most other methods mentioned, the FCM combines the fictitious domain idea with the benefits of high-order Finite Elements ( $p$ -FEM) [38]. Latest research results show that this new approach yields good results in the fields of linear elasticity [26, 11], topology optimization [12], geometrically nonlinear continuum mechanics [36], **adaptive mesh-refinement** [33, 34, 35], computational steering [41, 29], biomedical engineering [30, 40, 31] and convection diffusion problems [8, 6, 7].

Two major challenges arise following the idea of non-conforming discretizations: the correct numerical integration of the weak form and the appropriate enforcement of Dirichlet boundary conditions. For the first problem, an adaptive quadrature scheme is employed which captures the original domain during the integration process and has proven to work very well in the FCM context [11, 1]. For the second challenge, the concept of weak boundary conditions is utilized that was introduced in [24] for Laplace problems and in [3] for convection-diffusion and Navier-Stokes problems and has proven to yield good results in the framework of the FCM [36].

This paper aims to analyse the method's potential for multi-physical problems in the field of thermoelasticity. The presented research further addresses the weak enforcement of Dirichlet boundary conditions on non-conforming meshes **in the thermoelastic context**.

For this purpose, the governing equations of linear thermoelasticity and the essential ideas of the Finite Cell Method are recapitulated in the first half of this paper. ~~Nitsche's Method is introduced to weakly impose Dirichlet boundary conditions on non-conforming meshes.~~ Then, the concept of weak boundary conditions is outlined. The second part of the paper **assesses demonstrates** the quality of the numerical approximation with the help of an analytical benchmark and a practice-oriented example.

## 2. Theory of Linear Thermoelasticity

The objective of a thermoelastic analysis is to compute the deformation of an elastic body subjected to mechanical and thermal loadings. In a first step, this requires the computation of the temperature distribution. The resulting deformation can then be computed in a second step. The back-coupling effect of the displacement onto the temperature is neglected in the linearized formulation of thermoelasticity. Detailed information about this topic and the derivation of the governing equations are presented in [25]. This section recapitulates the final equations.

The elastic continuum is described by the physical domain  $\Omega_{phy}$ . Its domain boundary  $\partial\Omega_{phy}$  is composed of a Dirichlet and a Neumann boundary. Note that this boundary segmentation is not required to coincide for the thermal and the elastic computation. In the thermal case, the two boundary parts are denoted as  $\Gamma_D^{th}$  and  $\Gamma_N^{th}$ , respectively. In the elastic case,  $\Gamma_D^{el}$  and  $\Gamma_N^{el}$  are used as the respective label. In both cases, the two segments have to, however, recover the original boundary:

$$\Gamma_D \cup \Gamma_N = \partial\Omega_{phy} \quad \text{and} \quad \Gamma_D \cap \Gamma_N = \{\emptyset\}.$$

The temperature distribution  $\phi(\mathbf{x})$  follows from the stationary heat equation:

$$\nabla \cdot (\kappa \nabla \phi) - s = 0 \quad \text{in } \Omega_{phy} \tag{1a}$$

$$\phi = \hat{\phi} \quad \text{on } \Gamma_D^{th} \tag{1b}$$

$$\nabla \phi \cdot \mathbf{n} = \hat{q} \quad \text{on } \Gamma_N^{th}, \tag{1c}$$

with  $\kappa$ ,  $s$ , and  $\mathbf{n}$  being the thermal heat conduction coefficient, the heat source, and the outward pointing normal vector of the boundary, respectively. Furthermore,  $\hat{\phi}$  and  $\hat{q}$  denote the prescribed temperature on the Dirichlet boundary and the prescribed normal heat flux on the Neumann boundary, respectively.

The Duhamel-Neumann thermoelastic constitutive law (eq. (2b), cf. [32]) captures the influence of the temperature onto the mechanical continuum. The displacement  $\mathbf{u}(\mathbf{x})$  then follows from the governing equations of linear

thermoelasticity:

$$\nabla \cdot \boldsymbol{\sigma} + \mathbf{b} = \mathbf{0} \quad \text{in } \Omega_{phy} \quad (2a)$$

$$\boldsymbol{\sigma} = \mathbf{C} : (\boldsymbol{\varepsilon} - \boldsymbol{\varepsilon}^{th}) \quad \text{in } \Omega_{phy} \quad (2b)$$

$$\boldsymbol{\varepsilon} = \frac{1}{2} \cdot (\nabla \mathbf{u} + (\nabla \mathbf{u})^\top) \quad \text{in } \Omega_{phy} \quad (2c)$$

$$\boldsymbol{\varepsilon}^{th} = \gamma \cdot (\phi - \phi_0) \cdot \mathbf{I} \quad \text{in } \Omega_{phy} \quad (2d)$$

$$\mathbf{u} = \hat{\mathbf{u}} \quad \text{on } \Gamma_D^{el} \quad (2e)$$

$$\boldsymbol{\sigma} \cdot \mathbf{n} = \hat{\mathbf{t}} \quad \text{on } \Gamma_N^{el}, \quad (2f)$$

with  $\boldsymbol{\sigma}$ ,  $\mathbf{b}$ ,  $\mathbf{C}$ ,  $\boldsymbol{\varepsilon}$ ,  $\boldsymbol{\varepsilon}^{th}$ ,  $\gamma$ ,  $\phi_0$ ,  $\hat{\mathbf{u}}$  and  $\hat{\mathbf{t}}$  denoting the stress tensor, the applied mechanical volume load, the constitutive tensor, the strain tensor, the thermal strain tensor, the thermal expansion coefficient, the stress-free reference temperature, the prescribed displacements on the Dirichlet boundary, and the prescribed tractions on the Neumann boundary, respectively.

The later use of the Finite Element or the Finite Cell Method requires the transformation of the above equations into the weak form [44, 20]. The thermoelastic problem then reads

*Find  $\phi \in X^{th}$  and  $\mathbf{u} \in X^{el}$  such that*

$$\mathcal{B}^{th}(\phi, \delta\phi) = \mathcal{F}^{th}(\delta\phi) \quad \forall \delta\phi \in Y^{th} \quad (3a)$$

$$\text{and } \mathcal{B}^{el}(\mathbf{u}, \delta\mathbf{u}) = \mathcal{F}^{el}(\delta\mathbf{u}, \phi) \quad \forall \delta\mathbf{u} \in Y^{el}, \quad (3b)$$

with  $X^{th}$  and  $X^{el}$  denoting the space of admissible temperature and displacement functions, respectively.  $Y^{th}$  and  $Y^{el}$  label the spaces of admissible virtual temperature and displacement functions [38]. The individual terms

of the weak form read

$$\mathcal{B}^{th}(\phi, \delta\phi) = \int_{\Omega_{phy}} \nabla\delta\phi \cdot \kappa \cdot \nabla\phi \, d\Omega \quad (4a)$$

$$\mathcal{F}^{th}(\delta\phi) = \int_{\Omega_{phy}} \delta\phi \cdot s \, d\Omega + \int_{\Gamma_N^{th}} \delta\phi \cdot \hat{q} \, d\Gamma \quad (4b)$$

$$\mathcal{B}^{el}(\mathbf{u}, \delta\mathbf{u}) = \int_{\Omega_{phy}} \boldsymbol{\varepsilon}(\delta\mathbf{u}) : \mathbf{C} : \boldsymbol{\varepsilon}(\mathbf{u}) \, d\Omega \quad (4c)$$

$$\begin{aligned} \mathcal{F}^{el}(\delta\mathbf{u}, \phi) &= \int_{\Omega_{phy}} \delta\mathbf{u} \cdot \mathbf{b} \, d\Omega + \int_{\Gamma_N^{el}} \delta\mathbf{u} \cdot \hat{\mathbf{t}} \, d\Gamma \\ &+ \int_{\Omega_{phy}} \boldsymbol{\varepsilon}(\delta\mathbf{u}) : \mathbf{C} : \boldsymbol{\varepsilon}^{th}(\phi) \, d\Omega. \end{aligned} \quad (4d)$$

Note that the third term on the right-hand side of (4d) expresses the influence of the thermal field onto the elastic field. Therefore, it yields the coupling term that connects both physical fields on the domain  $\Omega_{phy}$ .

Although (3) naturally covers the Neumann boundary conditions (1c) and (2f), it does not include the Dirichlet boundary conditions (1b) and (2e). Instead, these constraints are met by an appropriate selection of the admissible functions spaces  $X^{th}$ ,  $X^{el}$ ,  $Y^{th}$ , and  $Y^{el}$ .

For a standard Finite Element analysis, the formulation of such function spaces poses no problem because the Finite Element mesh resolves the domain boundary. In contrast, Fictitious Domain Methods employ non-conforming meshes. Since the function spaces are then no longer defined on the physical domain, their formulation is no longer straightforward. This demands for a relaxation of the restriction on the admissible function spaces and an incorporation of the Dirichlet boundary conditions in the weak form.

Various approaches follow this weak enforcement strategy such as the Lagrange Multiplier and the Penalty Method [44, 43]. ~~Another possibility is Nitsche's Method, originally proposed for Laplace problems. A comparison naming the advantages and shortcomings of the three approaches is given in [17]. In this paper, Nitsche's Method is employed.~~ Another possibility is to adopt a method originally proposed for Laplace problems by Nitsche [24] and for convection-diffusion problems by Bazilevs and Hughes [3]. The major advantage of this approach is its inherent consistency, which ensures that the analytical solution of the strong problem (2) also solves the adopted weak problem ([13], [15], [2]). However, the method gives rise to a scalar

penalty parameter whose value has to be above a certain threshold to ensure the coercivity of the weak form. As described in [3, 13, 15, 24], this lower threshold depends on the mesh size, the polynomial degree and the material properties. Hence, the penalty parameter is problem dependent and [13, 15] suggest to solve a generalized eigenvalue problem to capture the lower threshold. However, their studies show that, due to the consistency of the method, choosing any other penalty value above this threshold has almost no influence on the numerical result. These findings are confirmed in the context of the FCM by Ruess *et al.* [31] and Schillinger *et al.* [36], who showed that also with an empirical choice of the parameter value, good results can be achieved. Therefore, this Nitsche-like approach is followed in this paper.

The Nitsche expressions constraining the temperature  $\phi$  on the Dirichlet boundary read

$$\begin{aligned} \mathcal{G}^{th}(\phi, \delta\phi) &= \int_{\Gamma_D^{th}} \delta\phi \cdot \beta^{th} \cdot \phi \, d\Gamma \\ &\quad - \int_{\Gamma_D^{th}} \delta(\nabla\phi) \cdot \mathbf{n} \cdot \kappa \cdot \phi \, d\Gamma \\ &\quad - \int_{\Gamma_D^{th}} \delta\phi \cdot \kappa \cdot \mathbf{n} \cdot (\nabla\phi) \, d\Gamma \end{aligned} \tag{5a}$$

$$\begin{aligned} \text{and } \mathcal{g}^{th}(\delta\phi) &= \int_{\Gamma_D^{th}} \delta\phi \cdot \beta^{th} \cdot \hat{\phi} \, d\Gamma \\ &\quad - \int_{\Gamma_D^{th}} \delta(\nabla\phi) \cdot \mathbf{n} \cdot \kappa \cdot \hat{\phi} \, d\Gamma, \end{aligned} \tag{5b}$$

with  $\beta^{th}$  being the non-negative penalty parameter described above. The weak enforcement of the boundary conditions of the elastic problem follow

in analogy:

$$\begin{aligned}
\mathcal{G}^{el}(\mathbf{u}, \delta\mathbf{u}) &= \int_{\Gamma_D^{el}} \delta\mathbf{u} \cdot \beta^{el} \cdot \mathbf{u} \, d\Gamma \\
&\quad - \int_{\Gamma_D^{el}} (\boldsymbol{\sigma}(\delta\mathbf{u}) \cdot \mathbf{n}) \cdot \mathbf{u} \, d\Gamma \\
&\quad - \int_{\Gamma_D^{el}} \delta\mathbf{u} \cdot (\boldsymbol{\sigma}(\mathbf{u}) \cdot \mathbf{n}) \, d\Gamma \\
\text{and } \mathcal{g}^{el}(\delta\mathbf{u}) &= \int_{\Gamma_D^{el}} \delta\mathbf{u} \cdot \beta^{el} \cdot \hat{\mathbf{u}} \, d\Gamma \\
&\quad - \int_{\Gamma_D^{el}} (\boldsymbol{\sigma}(\delta\mathbf{u}) \cdot \mathbf{n}) \cdot \hat{\mathbf{u}} \, d\Gamma.
\end{aligned}$$

The constitutive equation (2b) allows for a reformulation in terms of the primary variables  $\mathbf{u}$  and  $\phi$ :

$$\begin{aligned}
\mathcal{G}^{el}(\mathbf{u}, \delta\mathbf{u}) &= \int_{\Gamma_D^{el}} \delta\mathbf{u} \cdot \beta^{el} \cdot \mathbf{u} \, d\Gamma \\
&\quad - \int_{\Gamma_D^{el}} (\boldsymbol{\varepsilon}(\delta\mathbf{u}) : \mathbf{C} \cdot \mathbf{n}) \cdot \mathbf{u} \, d\Gamma \\
&\quad - \int_{\Gamma_D^{el}} \delta\mathbf{u} \cdot (\mathbf{n} \cdot \mathbf{C} : \boldsymbol{\varepsilon}(\mathbf{u})) \, d\Gamma \tag{6a}
\end{aligned}$$

$$\begin{aligned}
\text{and } \mathcal{g}^{el}(\delta\mathbf{u}, \phi) &= \int_{\Gamma_D^{el}} \delta\mathbf{u} \cdot \beta^{el} \cdot \hat{\mathbf{u}} \, d\Gamma \\
&\quad - \int_{\Gamma_D^{el}} (\boldsymbol{\varepsilon}(\delta\mathbf{u}) : \mathbf{C} \cdot \mathbf{n}) \cdot \hat{\mathbf{u}} \, d\Gamma \\
&\quad - \int_{\Gamma_D^{el}} \delta\mathbf{u} \cdot (\mathbf{n} \cdot \mathbf{C} : \boldsymbol{\varepsilon}^{th}(\phi)) \, d\Gamma. \tag{6b}
\end{aligned}$$

Note that the last summand in (6b) yields a new coupling term, which additionally connects the thermal and the elastic field on the Dirichlet boundary. Due to ~~Nitsche's Method~~ [the weak boundary conditions](#), the two physical fields are, therefore, not only coupled on the domain  $\Omega_{phy}$  but also on the Dirichlet boundary  $\Gamma_D$  [42].

Taking the [Nitsche constraining](#) extensions into account, the weak formulation of the linear thermoelastic problem changes to:

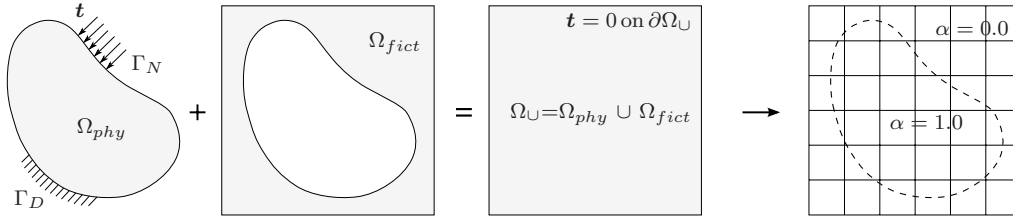


Figure 1: The Finite Cell idea: The physical domain  $\Omega_{phy}$  is embedded into the fictitious domain  $\Omega_{fict}$ . The resulting  $\Omega_{\cup}$  can be discretized easily which prevents complex mesh generation for  $\Omega_{phy}$ . The original problem is recovered by the localization factor  $\alpha$  [36].

Find  $\phi, \mathbf{u} \in H^1$  such that

$$\mathcal{B}^{th}(\phi, \delta\phi) + \mathcal{G}^{th}(\phi, \delta\phi) = \mathcal{F}^{th}(\delta\phi) + \mathcal{g}^{th}(\delta\phi) \quad (7a)$$

and

$$\mathcal{B}^{el}(\mathbf{u}, \delta\mathbf{u}) + \mathcal{G}^{el}(\mathbf{u}, \delta\mathbf{u}) = \mathcal{F}^{el}(\delta\mathbf{u}) + \mathcal{g}^{el}(\delta\mathbf{u}, \phi) \quad (7b)$$

$$\forall \delta\phi, \delta\mathbf{u} \in H^1,$$

where  $H^1$  denotes the Sobolev space.

Based on this formulation, the Finite Cell Method can be employed. The following chapter outlines the essential ideas of this approach.

### 3. The Finite Cell Method

As indicated in the introduction, the Finite Cell Method combines the ideas of Fictitious Domain Methods with those of high-order Finite Elements ( $p$ -FEM) [38]. The method aims to reduce the effort required for mesh generation while yielding high-order convergence rates on non-conforming meshes. It was first introduced for 2D problems in [26] and extended to 3D in [11]. Following these publications, this section recapitulates the essential ideas of the method.

#### 3.1. Basic Concept

The Finite Cell Method inherits the FEM idea to find the “best approximation” of an analytical solution in a finite dimensional ansatz space  $V^h \subset H^1(\Omega_{phy})$  [20]. This is achieved by representing the numerical solution as a linear combination of shape functions that span  $V^h$ . The  $p$ -version of

the Finite Element Method uses integrated Legendre polynomials as shape functions [38]. With this representation of the numerical solution, the task of finding the best approximation yields a system of linear equations

$$\mathbf{K}\mathbf{a} = \mathbf{f}$$

that has to be solved for  $\mathbf{a}$  aggregating the coefficients of the linear combination. How the system matrix  $\mathbf{K}$  and the right-hand side vector  $\mathbf{f}$  follow from the weak form is, for example, illustrated in [44, 20, 38].

In contrast to the standard FE-approach, the Finite Cell Method utilizes the fictitious domain concept. This embeds the possibly complex physical domain  $\Omega_{phy}$  in a fictitious domain  $\Omega_{fict}$ . The FCM then solves the boundary value problem on their simply shaped union  $\Omega_{\cup}$  (cf. Figure 1) while recovering the original domain on the integration level by the localization factor

$$\alpha(\mathbf{x}) = \begin{cases} 1 & \text{if } \mathbf{x} \in \Omega_{phy} \\ 0 & \text{if } \mathbf{x} \in \Omega_{fict}. \end{cases} \quad (8)$$

This additional scalar field allows to reformulate the bilinear form (4a) in terms of  $\Omega_{\cup}$ :

$$\begin{aligned} \mathcal{B}^{th}(\phi, \delta\phi) &\stackrel{(4a)}{=} \int_{\Omega_{phy}} \nabla\delta\phi \cdot \kappa \cdot \nabla\phi \, d\Omega \\ &= \int_{\Omega_{phy}} \nabla\delta\phi \cdot \kappa \cdot \nabla\phi \, d\Omega \\ &\quad + \int_{\Omega_{fict}} 0 \cdot \nabla\delta\phi \cdot \kappa \cdot \nabla\phi \, d\Omega \\ &\stackrel{(8)}{=} \int_{\Omega_{\cup}} \alpha \cdot \nabla\delta\phi \cdot \kappa \cdot \nabla\phi \, d\Omega. \end{aligned} \quad (9a)$$

The remaining expressions of (4) follow in analogy:

$$\mathcal{F}^{th}(\delta\phi) = \int_{\Omega_{\cup}} \alpha \cdot \delta\phi \cdot s \, d\Omega + \int_{\Gamma_N^{th}} \delta\phi \cdot \hat{q} \, d\Gamma \quad (9b)$$

$$\mathcal{B}^{el}(\mathbf{u}, \delta\mathbf{u}) = \int_{\Omega_{\cup}} \alpha \cdot \boldsymbol{\varepsilon}(\delta\mathbf{u}) : \mathbf{C} : \boldsymbol{\varepsilon}(\mathbf{u}) \, d\Omega \quad (9c)$$

$$\begin{aligned} \mathcal{F}^{el}(\delta\mathbf{u}, \phi) &= \int_{\Omega_{\cup}} \alpha \cdot \delta\mathbf{u} \cdot \mathbf{b} \, d\Omega + \int_{\Gamma_N^{el}} \delta\mathbf{u} \cdot \mathbf{t} \, d\Gamma \\ &\quad + \int_{\Omega_{\cup}} \alpha \cdot \delta\boldsymbol{\varepsilon} : \mathbf{C} : \boldsymbol{\varepsilon}^{th}(\phi) \, d\Omega. \end{aligned} \quad (9d)$$

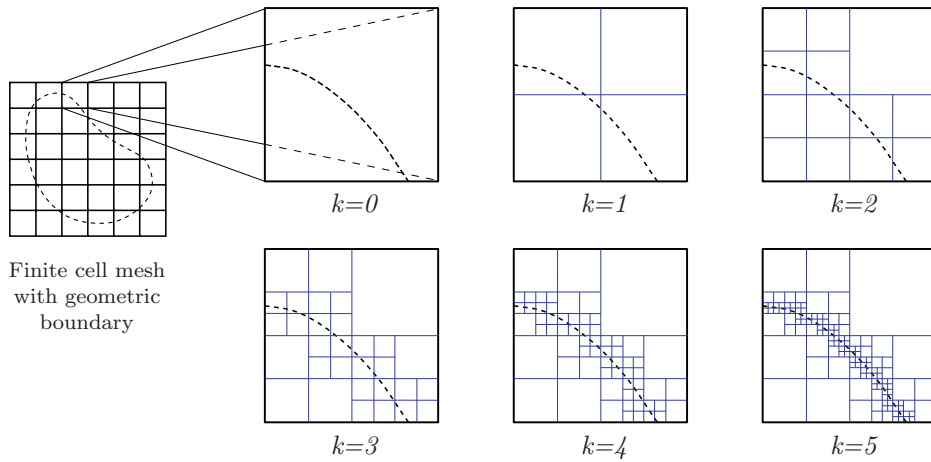


Figure 2: Domain integration scheme: The physical domain is captured on a  $k$ -times recursively refined integration mesh [36]

This idea circumvents the discretization of the possibly complex original geometry and allows for meshing the simply shaped domain  $\Omega_{\cup}$  instead. The resulting non-conforming high-order elements are denoted as cells giving the method its name (cf. Figure 1).

Although the Finite Cell idea is rather simple, its implementation faces some challenges. In particular, the domain integration and the boundary conditions require special care. These two aspects shall be discussed in more detail.

**Remark:** Since the finite cell mesh is rather coarse and not aligned with the physical domain, a certain smoothness of the solution has to be assumed. In particular, singularities caused by the domain geometry and/or boundary conditions could not be captured correctly by the coarse discretization. As described in [37], a successive  $h$ -refinement towards the point of singularity is required to better capture the solution and to shield the rest of the domain sufficiently from the influence of the singularity. Following this idea, Schillinger and co-workers [33, 34, 35] recently extended the Finite Cell idea by a hierarchical  $hp$ - $d$  refinement strategy, where, in analogy to the integration scheme, also the actual mesh is adaptively refined. This extension allows to capture non-smooth solutions, as well.

### 3.1.1. Domain Integration Scheme

As shown in the previous section, the parameter  $\alpha$  allows to identify the physical domain  $\Omega_{phy}$  within the embedding fictitious domain  $\Omega_{fict}$  during integration. Unfortunately, this yields discontinuous integrands in (9) which inhibits the straightforward use of the Gaussian quadrature rule [28, 20]. Instead, the FCM requires special integration schemes to resolve the discontinuous integrand. A detailed discussion on different approaches is presented in [1]. The general ideas are outlined here.

One possibility to capture the discontinuity is to adjust the weighting factors of the individual Gaussian integration points. This approach can be elaborated by an additional modification of the Gauss-point positions.

A different idea is to resolve the discontinuity via a triangulation of  $\Omega_{phy}$ . XFEM and Level Set approaches commonly employ this strategy since it is rather simple to implement when using linear shape functions [23, 10]. Also high order triangulations are possible, and optimal convergence up to order three can be obtained as shown in [9]. However, for higher polynomial degrees, the complexity of the approach increases. It also contradicts the aim of the FCM to avoid complex meshing, which is why it is not employed here.

Instead, the FCM applies a recursive refinement strategy to resolve the physical domain on a locally adapted integration mesh (cf. Figure 2). In addition to the simple quad- or oct-tree data structure, this approach offers the advantage that it does not require an explicit formulation of the boundary. Only an inside/outside test has to be performed for the corner points of each integration cell. This can, for example, be done using a STL<sup>1</sup>-based domain description in conjunction with a k-d-tree library [5]. Note that the integration approach does not introduce additional degrees of freedom (dofs) since the Finite Cell discretization remains unchanged. Therefore, the size of the final system of equations does not increase.

### 3.1.2. Imposing Boundary Conditions on Non-conforming Meshes

Since the Finite Cell mesh does not resolve the physical domain, also the boundary conditions require special consideration.

Non-homogeneous Neumann conditions require the integration of the respective surface integrals in (4b) and (4d) over the boundary  $\Gamma_N$ . This demands for a surface discretization. A simple possibility to generate these

---

<sup>1</sup>stereolithography

boundary meshes is an export of the surface description from a CAD<sup>2</sup>program into a STL-file. As for the domain discretization, this additional mesh has no effect on the Finite Cell discretization and does not introduce any additional degrees of freedom.

Dirichlet boundary conditions are treated in analogy to the Neumann conditions by the integration of the Nitsche extension terms (5) and (6) on the basis of the described surface discretization.

### 3.2. The Finite Cell Method for Linear Thermoelasticity

As discussed in Section 2, a thermoelastic analysis addresses the interaction between a thermal and an elastic field. This two-field coupling carries over to the discretization:

$$\begin{bmatrix} \mathbf{K}^{th} & \mathbf{C}^{th} \\ \mathbf{C}^{el} & \mathbf{K}^{el} \end{bmatrix} \begin{bmatrix} \phi \\ \mathbf{u} \end{bmatrix} = \begin{bmatrix} \mathbf{f}^{th} \\ \mathbf{f}^{el} \end{bmatrix},$$

with  $\mathbf{K}^{th}$  and  $\mathbf{K}^{el}$  being the thermal and elastic system matrices, respectively. The solution vectors  $\phi$  and  $\mathbf{u}$  denote the coefficients of the respective linear combinations. The vectors  $\mathbf{f}^{th}$  and  $\mathbf{f}^{el}$  follow from the discretization of the right-hand side of the weak form (7).  $\mathbf{C}^{th}$  and  $\mathbf{C}^{el}$  are the coupling matrices, which describe the field interaction.

Since this paper presents a first solution step of this general problem by focusing on linear thermoelasticity, the back-coupling influence of the displacement  $\mathbf{u}$  onto the temperature  $\phi$  can be neglected. The coupling matrix  $\mathbf{C}^{th}$  can, therefore, be taken out of consideration. This simplifies the system as follows:

$$\begin{bmatrix} \mathbf{K}^{th} & \mathbf{0} \\ \mathbf{C}^{el} & \mathbf{K}^{el} \end{bmatrix} \begin{bmatrix} \phi \\ \mathbf{u} \end{bmatrix} = \begin{bmatrix} \mathbf{b}^{th} \\ \mathbf{b}^u \end{bmatrix}. \quad (10)$$

In literature, monolithic and partitioned solution strategies are discussed for such problems [14]. The first approach solves the above system as a whole. A partitioned scheme, which is chosen here, transfers the problem into an explicit form and solves it in two steps:

$$\text{First solve } \mathbf{K}^{th} \phi = \mathbf{b}^{th}. \quad (11a)$$

$$\text{Then solve } \mathbf{K}^{el} \mathbf{u} = \mathbf{b}^{el} - \mathbf{C}^{el} \phi. \quad (11b)$$

---

<sup>2</sup>Computer Aided Design

Following this approach, the coupling between the two fields reduces to exchange data between the two solution steps. As discussed in Section 2, the two fields are coupled on the physical domain by (4d) and on the Dirichlet boundary by (6b). Therefore, the algorithm for the solution of the linear thermoelasticity problem includes the following steps:

1. Pre-processing steps
  - (a) Export of the geometric model from the CAD program into a STL-File.
  - (b) Decision about a fictitious domain. Typically, a bounding box is chosen.
  - (c) Discretization of  $\Omega_{\cup}$  with a simple Cartesian mesh.
  - (d) Setup of surface meshes for the boundary conditions.
2. Solution steps
  - (a) Solve (11a) for  $\phi$
  - (b) Extract coupling data on  $\Omega_{phy}$  and  $\Gamma_D$  from solution
  - (c) Solve (11b) for  $\mathbf{u}$
3. Post-processing

## 4. Numerical Examples

The two previous sections introduced the governing equations of linear thermoelasticity and the essential ideas of the Finite Cell Method. ~~This part of the paper assesses the applicability~~ This part of the paper is concerned with the assessment of the applicability of the FCM for linear thermoelastic problems with the help of two 2D, plane stress examples. The first problem is an academic benchmark which allows to study the convergence properties of the method. The second example is practice-oriented and ~~assesses demonstrates~~ the approximation qualities of the FCM on a complex physical domain.

### 4.1. Analytical Benchmark

The following example aims to study the convergence properties of the Finite Cell Method in the context of linear thermoelasticity. For this purpose, the method is employed to simulate the thermoelastic state of the 2D ring plate shown in Figure 3.

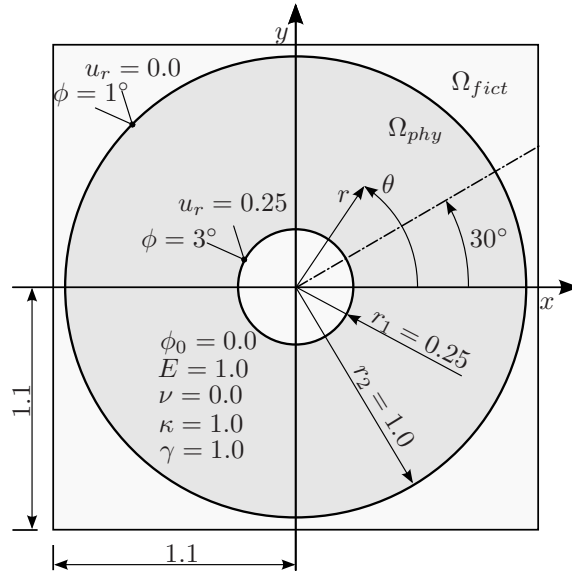
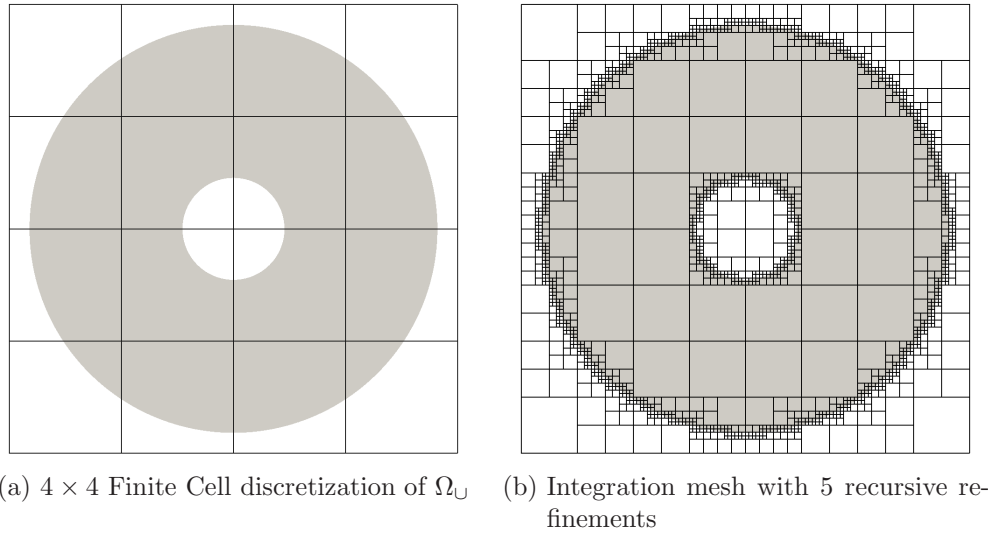


Figure 3: Geometrical and constitutive setup of the ring benchmark



(a)  $4 \times 4$  Finite Cell discretization of  $\Omega_U$  (b) Integration mesh with 5 recursive refinements

Figure 4: Domain discretization

#### 4.1.1. Example Setup

As depicted, the temperature on the in- and outside of the ring is set to  $3^\circ$  and  $1^\circ$ , respectively. With the help of the given thermal material properties

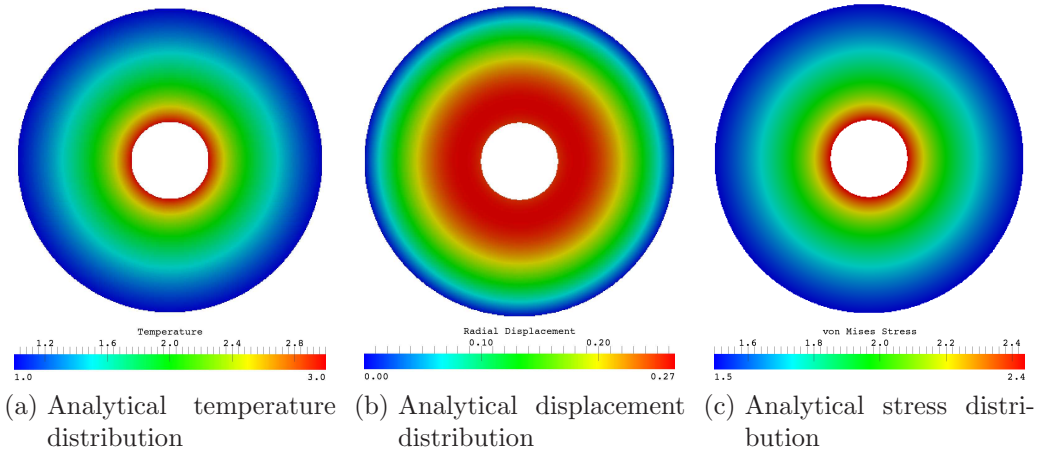


Figure 5: Analytical solutions

(cf. Figure 3), the analytical temperature distribution reads

$$\phi(r) = 1 - \frac{\ln(r)}{\ln(2)}, \quad (12)$$

with  $r$  denoting the radial distance. The energy norm [20] of the temperature distribution yields

$$\begin{aligned} \|\phi\|_E^2 &= \frac{1}{2} \mathcal{B}^{th}(\phi, \phi) \stackrel{(4a)}{=} \frac{1}{2} \int_{\Omega_{phy}} \nabla \phi \cdot \kappa \cdot \nabla \phi \, d\Omega \\ &\stackrel{(12)}{=} \pi \cdot \frac{4}{\ln(4)} \approx 9.064720284. \end{aligned} \quad (13)$$

In addition to the thermal loading (12), the ring is displaced by 0.25 units<sup>3</sup> in radial direction on the inside boundary whereas the outer boundary is fixed. With the mechanical material properties given in Figure 3, the displacement of the ring reads

$$u_r(r) = -\frac{r \ln(r)}{2 \ln(2)} \quad (14a)$$

$$u_\theta(r) = 0, \quad (14b)$$

---

<sup>3</sup>Although this large deformation of the ring violates the assumption of small displacements for linear elasticity, the boundary conditions are still valid for this academic benchmark example since it aims to ~~asses~~ **demonstrate** the method's potential in the context of linear thermoelasticity.

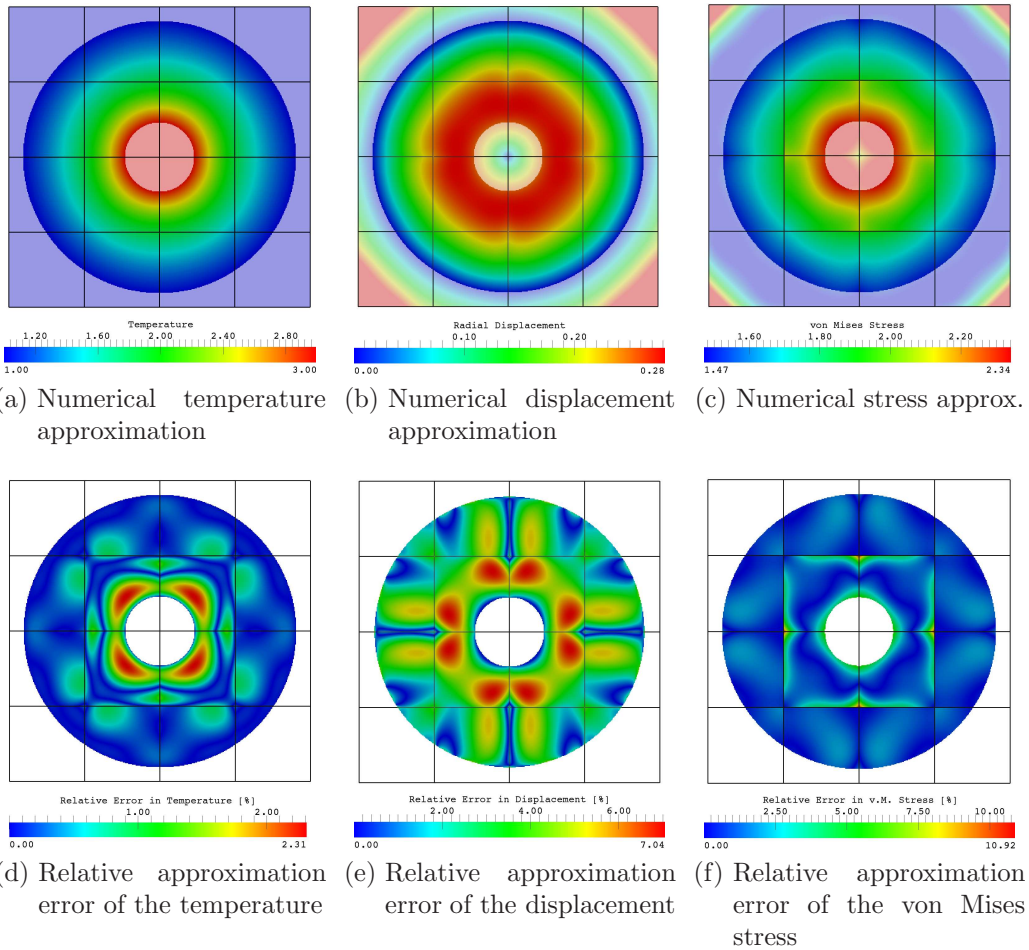


Figure 6: Numerical results computed with shape functions of polynomial degree  $p = 3$  (105 and 210 dofs for the temperature and displacement, respectively) (Remark: The error on the outer boundary in Figure 6e is not depicted since any deviation from the analytical value zero would result in a infinite relative error)

with  $r$  and  $\theta$  denoting the radial and angular coordinates, respectively. The

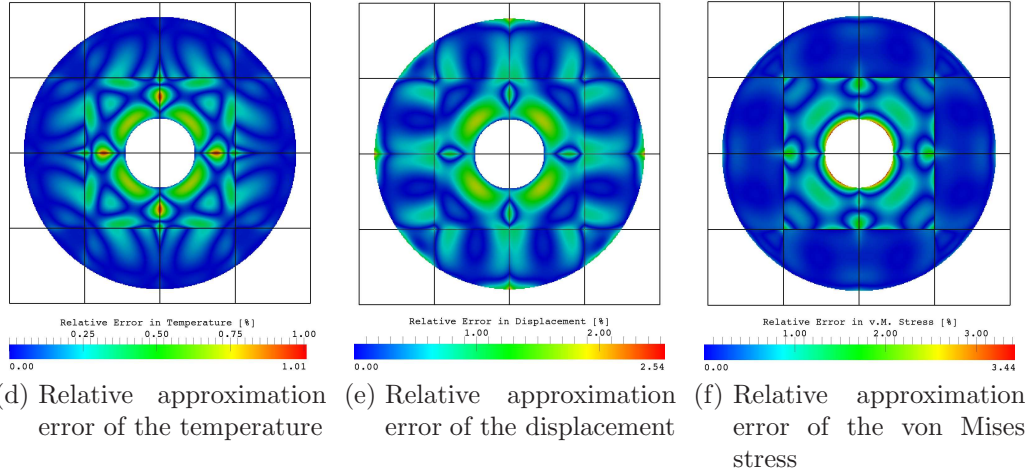
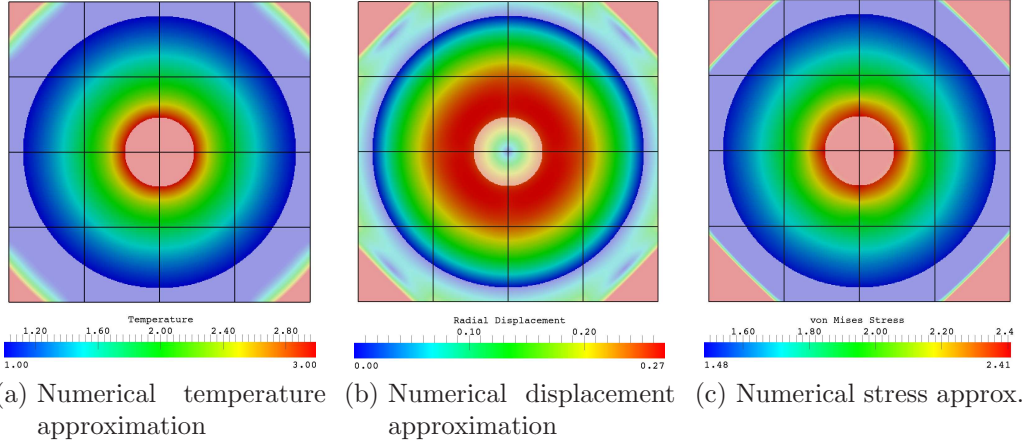


Figure 7: Numerical results computed with shape functions of polynomial degree  $p = 5$  (233 and 466 dofs for the temperature and displacement, respectively) (Remark: The error on the outer boundary in Figure 7e is not depicted since any deviation from the analytical value zero would result in a infinite relative error)

corresponding strains in polar coordinates read [32]

$$\varepsilon_r(r) = \frac{\partial u_r}{\partial r} = -\frac{1}{2} \frac{\ln(r) + 1}{\ln(2)} \quad (15a)$$

$$\varepsilon_\theta(r) = \frac{1}{r} \frac{\partial u_\theta}{\partial \theta} + \frac{u_r}{r} = -\frac{1}{2} \frac{\ln(r)}{\ln(2)} \quad (15b)$$

$$\varepsilon_{r\theta}(r) = \frac{1}{2} \left( \frac{1}{r} \frac{\partial u_r}{\partial \theta} + \frac{\partial u_\theta}{\partial r} - \frac{u_\theta}{r} \right) = 0. \quad (15c)$$

According to Hooke's law of plane stress in polar formulation [32], the following mechanical stress distribution results:

$$\begin{aligned}\sigma_r(r) &= \frac{E}{1-\nu^2} [\varepsilon_r + \nu\varepsilon_\theta - (1+\nu)\gamma(\phi - \phi_0)] \\ &= \varepsilon_r(r) - \phi(r)\end{aligned}\tag{16a}$$

$$\begin{aligned}\sigma_\theta(r) &= \frac{E}{1-\nu^2} [\varepsilon_\theta + \nu\varepsilon_r - (1+\nu)\gamma(\phi - \phi_0)] \\ &= \varepsilon_\theta(r) - \phi(r)\end{aligned}\tag{16b}$$

$$\sigma_{r\theta}(r) = \frac{E}{1+\nu}\varepsilon_{r\theta} = 0.\tag{16c}$$

The energy norm of the given displacement distribution yields

$$\begin{aligned}\|\mathbf{u}\|_E^2 &= \frac{1}{2}\mathcal{B}^{el}(\mathbf{u}, \mathbf{u}) \stackrel{(4c)}{=} \frac{1}{2} \int_{\Omega_{phy}} \boldsymbol{\varepsilon} : \mathbf{C} : \boldsymbol{\varepsilon} \, d\Omega \\ &\stackrel{(14)}{=} -\frac{\pi}{128} \left( 8 - \frac{15}{\ln(2)^2} \right) \approx 5.699176662 \cdot 10^{-1}.\end{aligned}\tag{17}$$

To numerically approximate these analytical distributions, the physical domain  $\Omega_{phy}$  is embedded in a square domain  $\Omega_U = [-1.1, 1.1]^2$  (cf. Figure 3), which is then discretized by a  $4 \times 4$  Finite Cell mesh (cf. Figure 4a). Based on an analytical description of the ring geometry, a recursive refinement strategy recovers the physical domain on the integration level (Figure 4b). In addition to these domain discretizations, the Dirichlet boundary conditions require a separate surface mesh. For this purpose, 1000 line segments approximate the curved boundaries by a fine polygon. The value of the penalty parameter is chosen empirically.  $\beta^{th}$  is set to  $10^4$ , and for  $\beta^{el}$  a value of  $10^3$  is chosen.

#### 4.1.2. Results and Discussion

The Finite Cell approximations resulting from the described numerical setup are depicted in Figure 6. The comparison to the analytic solutions (Figure 5) shows that, even with low order polynomials of degree 3, the FCM captures the temperature and displacement correctly. In particular, the results show no deviation on the boundary. The numerical solution also represents the stress state without major faults. Figure 7 shows that an increase of the polynomial degree leads to a significant reduction of the approximation error. Especially, mesh artifacts vanish as the comparison of

Figure 6b and 7b shows. The depicted relative errors of about 1 – 3% verify the quality of the numerical results.

The distribution of the relative error reveals that the deviations of all three results concentrate in the four inner cells. Especially for the stress approximation, the error in the outer cells is significantly lower than in the inner cells. The reason for this characteristic is the mutual influence of the four inner cells that constrain the extension of the numerical solution into the internal void. In contrast, the ansatz of the outer cells can extend freely, which allows for a better approximation of the analytical solution. Comparing Figure 6f and 7f shows that an increase of the polynomial degree yields a lower and more equally distributed approximation error in the four inner cells.

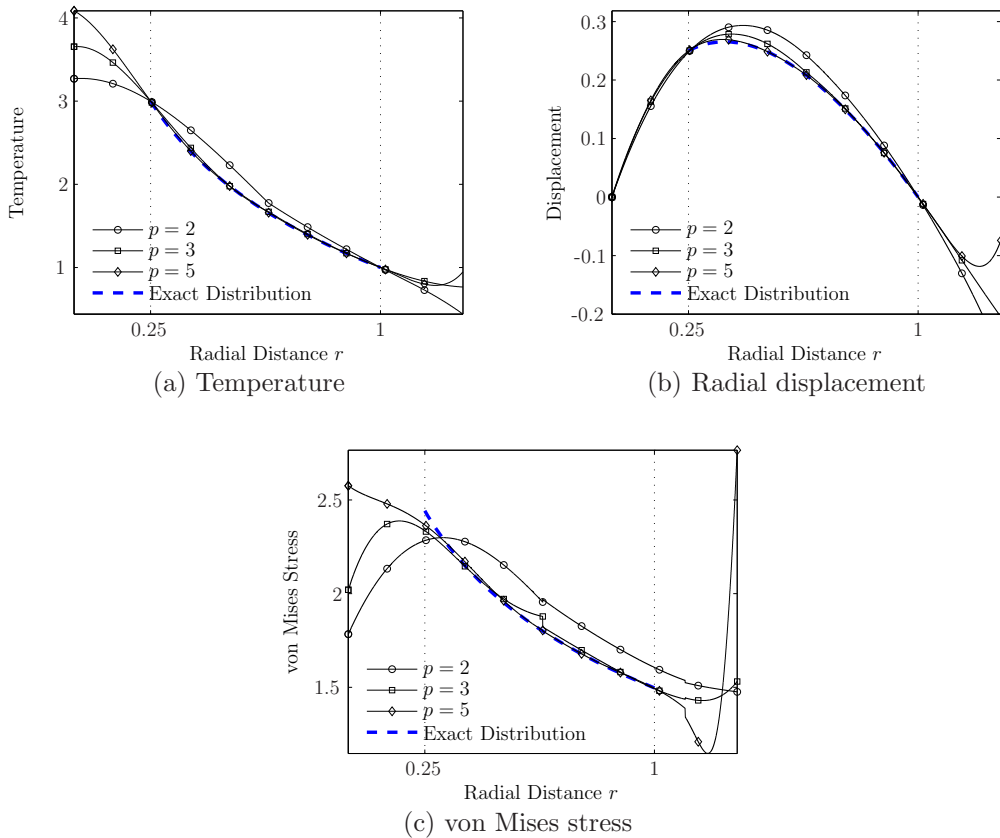


Figure 8: Comparison of the numerical approximations and the analytical solutions along the  $30^\circ$  cut-line for different polynomial degrees

For a detailed assessment of the approximation, Figure 8 depicts the numerical results along a  $30^\circ$  cut-line. The comparison to the exact solution verifies a good compliance of the approximation inside the physical domain  $r \in [0.25, 1]$ . On the boundary, the approximations meet the Dirichlet conditions and smoothly extend into the fictitious domain without oscillations. Note that the graphs reveal an error concentration inside the physical domain in conjunction with a high compliance of the boundary values. This discrepancy is especially pronounced for lower polynomial degrees and results from the high values chosen for  $\beta$  that penalize any deviation on the boundary.

The comparison also shows that the numerical approximations converge against the analytical solutions when increasing the polynomial degree  $p$ . Especially, the jumps in the stress distribution at the element crossings decrease. For  $p = 5$ , no major deviations in the stress results can be observed.

The influence of the polynomial degree  $p$  is assessed in more detail by a  $p$ -convergence of the error in the energy norm [11]:

$$\|e_\phi\|_E = \sqrt{\frac{|\|\phi\|_E^2 - \|\phi_{num}\|_E^2|}{\|\phi\|_E^2}} \cdot 100\%$$

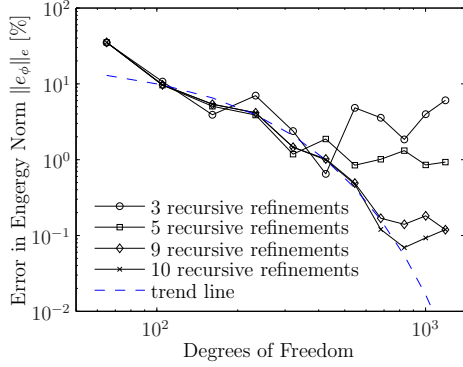
and

$$\|e_{\mathbf{u}}\|_E = \sqrt{\frac{|\|\mathbf{u}\|_E^2 - \|\mathbf{u}_{num}\|_E^2|}{\|\mathbf{u}\|_E^2}} \cdot 100\%.$$

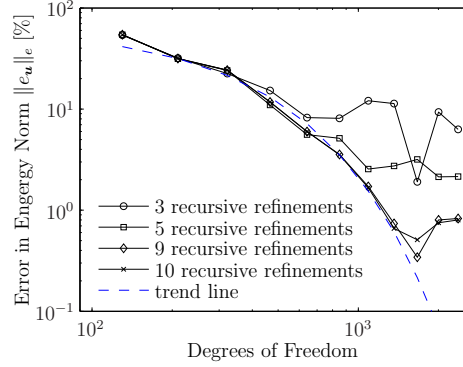
Figure 9 depicts the evolution of this error measure against the degrees of freedom. Different numbers of recursive mesh refinements are compared to investigate the influence of integration accuracy.

The convergence curves show that 3 recursive refinements do not resolve the physical domain with sufficient precision. The integration error dominates the numerical accuracy which results in low convergence rates. An increase of refinements reduces this influence and allows for higher accuracy. Nevertheless, the convergence flattens off at an accuracy level of about 0.1 – 1%. The mismatch between the numerical representation of the domain and its boundary is assumed to cause this behaviour and will be addressed in upcoming research. However, at an error of this level, the energy norm differs at the third or fourth decimal place, only. Typically, this accuracy is more than sufficient for engineering practice.

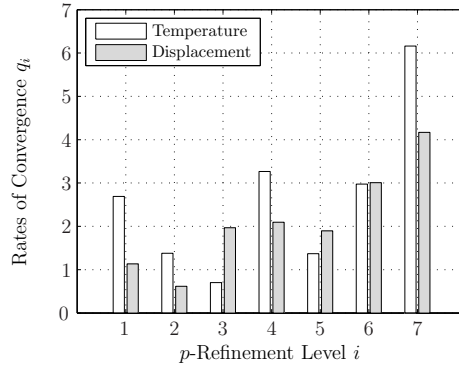
~~A study of the convergence rates shall conclude the result analysis. For this purpose,~~ To analyse the convergence characteristic in more detail, the



(a)  $p$ -convergence of temperature approximation achieved with different number of recursive refinements during integration



(b)  $p$ -convergence of displacement approximation achieved with different number of recursive refinements during integration



(c) Rates of Convergence on a 10 times recursively refined integration mesh

Figure 9:  $p$ -convergence study in the energy error norm for  $p = 2, 3, \dots, 12$

convergence rates are computed [37]:

$$q_i = -\frac{\log\left(\frac{\|e\|_E^{i+1}}{\|e\|_E^i}\right)}{\log\left(\frac{n^{i+1}}{n^i}\right)},$$

with  $\|e\|_E^i$  denoting the energy error and  $n^i$  denoting the number of unknowns in the  $i^{\text{th}}$  refinement step. Figure 9c depicts the improvement rates of the first seven steps.

The graph reveals that, at the beginning, the increase of  $p$  yields convergence rates of up to 2.7. In a traditional  $h$ -refinement, these improvements

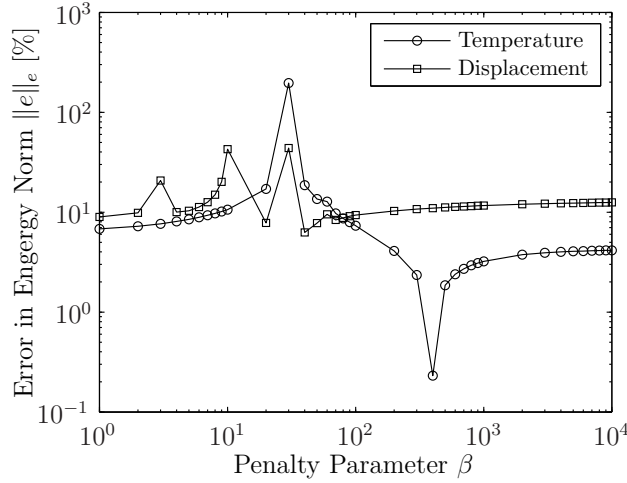


Figure 10: Influence of the penalty parameter  $\beta$  on the error in the energy norm on a 10 times recursively refined integration mesh with  $p = 5$ .

correspond to convergence rates of order 5 since, in two dimensions,  $n$  scales quadratically with the element size  $h$ . Therefore, the  $p$ -refinement achieves super-algebraic convergence. Above that, the graph shows an increase of the convergence rates. This indicates a pre-asymptotic exponential convergence for both fields. To visualize this convergence characteristic, an exponential interpolation between two empirically chosen points is depicted as a trend line in Figure 9a and 9b. ~~This comparison verifies that the head and tail of the convergence curves meet the exponential rates. However, the convergence drops, in between. The empirical choice of the penalty value  $\beta$  causes this non-monotonic behaviour.~~

~~The large influence of this parameter is depicted in Figure 10. In a certain range, a minor adjustment of  $\beta$  has significant effects on the error in the energy norm whereas, in other ranges, the influence is negligible. The  $\beta$  study shows that the penalty values for this benchmark were chosen from the latter part of the spectrum. For low order methods, the value of  $\beta$  can be approximated to achieve optimal convergence rates. The influence of this numerical parameter in the framework of the FCM is subject to current research.~~

~~Nevertheless, the partially exponential characteristic shows that this main quality assessment of high order methods can be achieved in context of linear thermoelasticity on non-conforming meshes when combining the FCM with Nitsche's Method.~~

Concluding this section, the influence of the penalty parameter value is analysed in Figure 10. As described in Section 2, the value of  $\beta$  has to be chosen above a lower threshold that ensures coercivity of the weak form. The depicted  $\beta$ -study shows that these critical values are  $4 \cdot 10^2$  for the thermal and  $4 \cdot 10^1$  for the elastic problem. The penalty values chosen for this benchmark example are therefore above the lower threshold and thus the coercivity of the weak form is ensured.

#### 4.2. Heat Exchanging Device

In contrast to the simply shaped ring benchmark, the following example aims to approximate the thermoelastic state of the heat exchanging device depicted in Figure 11. The results of the Finite Cell Method are compared to a Finite Element solution.

##### 4.2.1. Example Setup

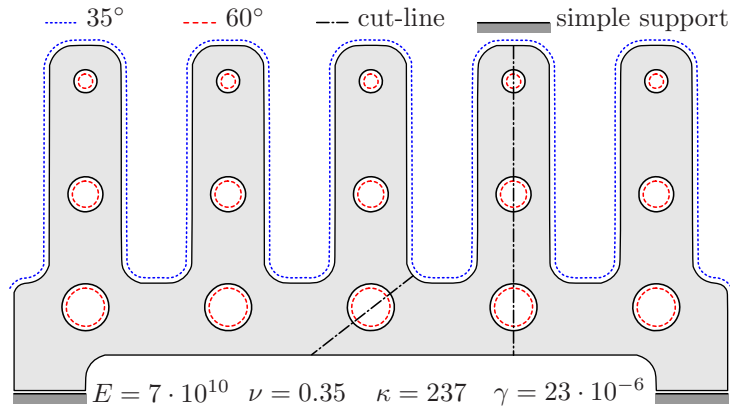


Figure 11: Setup of heat exchanging device

Inside the boreholes, a hot medium heats the device to  $60^\circ$ . A surrounding medium establishes a temperature of  $35^\circ$  on the outside.

To simulate the resulting temperature distribution, the Finite Element Method requires a conform meshing of the actual physical domain (cf. Figure 12a). In case of the Finite Cell Method, this complex discretization is avoided by embedding the physical domain in a simply shaped bounding box (cf. Figure 12b).

Since the conforming discretization resolves geometric features on mesh level, quadratic shape functions are sufficient to capture the solution characteristics. This discretization yields about 57,000 dofs for the temperature

simulation and almost 130,000 dofs for the displacement approximation, respectively. On the coarse Finite Cell mesh, 8 recursive refinements capture geometric details during integration using a STL-based domain description.

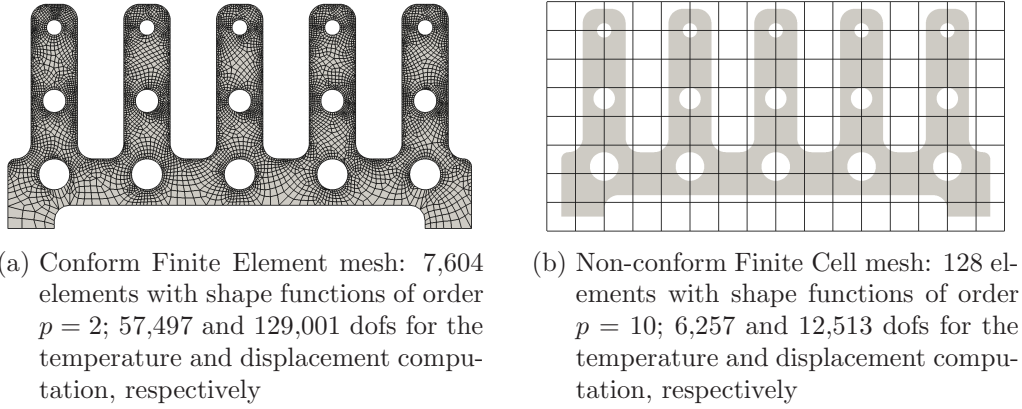


Figure 12: Domain discretization

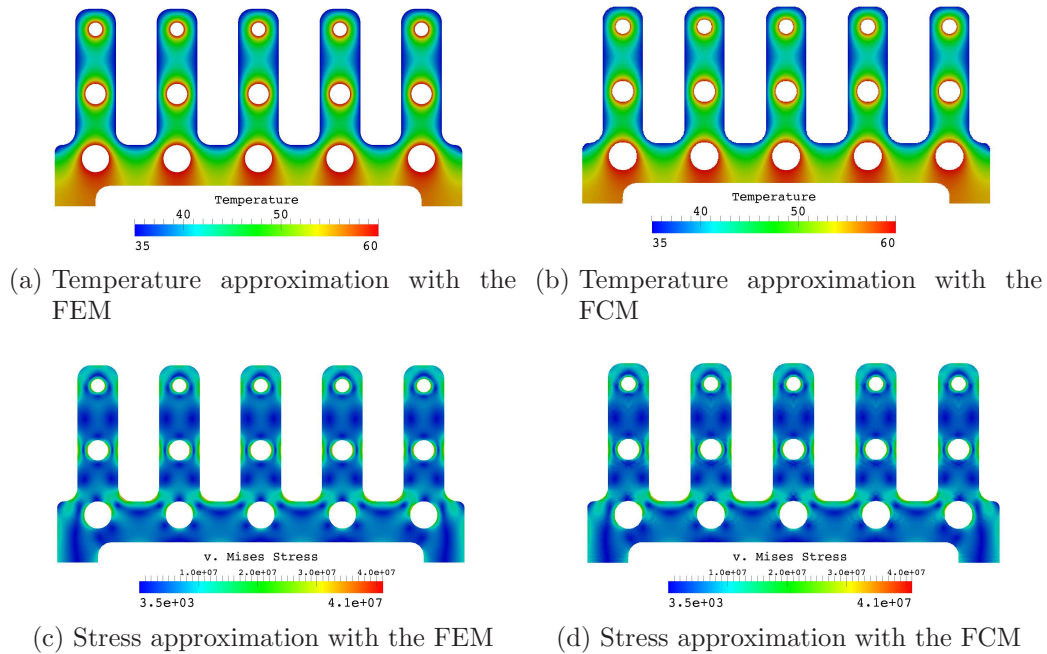


Figure 13: Comparison of the temperature and stress approximation with the FEM and the FCM

To represent the solution correctly, high order polynomials of degree  $p = 10$  are used as shape functions in the Finite Cell computations. Nevertheless, due to the coarse mesh, the number of unknowns in the Finite Cell simulation is significantly lower than in the Finite Element case. To avoid numerical problems while solving the system of equations, the value of the localization factor  $\alpha$  is not set to zero but to  $10^{-15}$ .

As for the ring benchmark, a fine polygon discretizes the boundary. For the temperature approximation, a penalty value of  $10^5$  is chosen empirically. In the displacement case,  $\beta^{el}$  is set to  $10^3$ . Fixing one node along the symmetrical axis in horizontal direction avoids rigid body motions.

#### 4.2.2. Results and Discussion

Based on the outlined numerical setup, both methods can approximate the temperature distribution. Figure 13 depicts the two results. The comparison shows that the range as well as the distribution of the both approximations match. Figure 14a extracts the results along the vertical cut-line depicted in Figure 11. The comparison proves that the results of the two numerical methods match inside of the actual physical domain. On the boundary, the Finite Cell solution meets the Dirichlet conditions and smoothly extends into the fictitious domain without oscillations. This confirms the findings of the previous example.

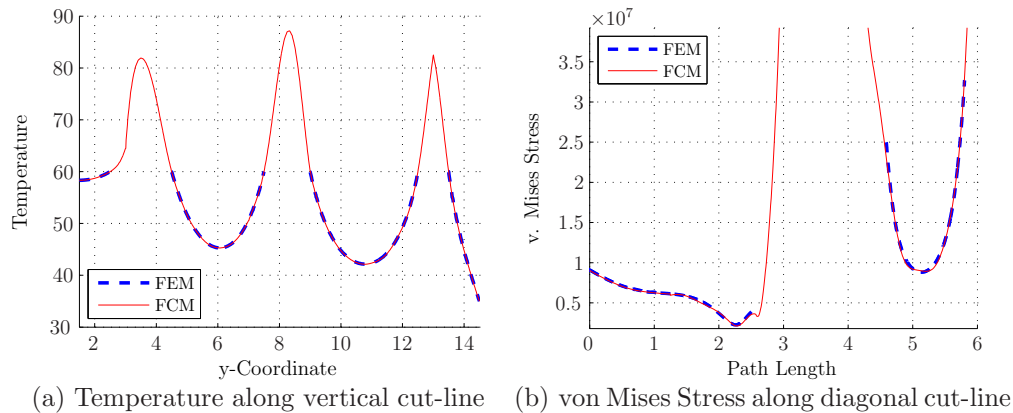


Figure 14: Comparison of the temperature and stress approximation along cut-lines

With the results of the temperature approximation at hand, the defor-

mation of the device is computed. Figure 13c and 13d depict the mechanical stress resulting from this thermal loading. As for the temperature, the results of both methods match in their range and distribution. In particular, the position of stress concentrations correspond. Figure 14b extracts the results along the diagonal cut line depicted in Figure 11. The comparison proves that also the stress approximations of both methods coincide within the physical domain. In particular, the Finite Cell Method even captures the stress concentrations at both reentrant corners correctly.

Together, these findings verify the applicability of the FCM to solve complex thermoelastic problems on non-conforming meshes.

## 5. Summary, Conclusion, and Outlook

This paper aims to solve linear thermoelastic problems in the high-order, fictitious domain framework of the Finite Cell Method. For this purpose, the first half of the article recapitulated the governing equations of linear thermoelasticity and the essential ideas of the FCM. The explanation focused on how Dirichlet boundary conditions of the coupled problem can be imposed on non-conforming meshes. It was shown that this requires an integration of the Dirichlet boundary conditions into the weak problem formulation and Nitsche's Method was introduced for this purpose. Applying this idea to the multi-physical problem of linear thermoelasticity gave rise to a new coupling term which connects the two fields additionally on the Dirichlet boundary.

The second half of this paper analysed the approximation quality of the FCM with the help of two examples. The studies verified that, even on complex physical domains, the temperature, the displacement as well as the stress distributions can be approximated with high accuracy. Also the boundary conditions could be imposed correctly on non-conforming meshes. For the analytical benchmark example, super-algebraic convergence rates in the energy norm could be observed and, partially, even exponential characteristics were achieved.

These findings prove that the FCM in conjunction with Nitsche's ideas can be applied for high order simulations of linear thermoelastic problems on non-conforming meshes. This verifies the applicability of the FCM for multi-physical problems.

~~In upcoming research, this aspect will be explored by addressing non-linear thermoelastic coupling as well as transient problems. Furthermore, three dimensional examples will follow.~~

The research presented in this paper focuses on smooth, stationary, linear thermoelastic problems in two dimensions. In upcoming research, it is planned to study the method's potential in the context of transient, non-linear thermoelastic coupling and to also address three-dimensional examples. Furthermore, the research will be extended to non-smooth thermoelastic problems utilizing the hierarchical *hp-d* refinement strategy, recently introduced by Schillinger *et al.* [33, 34, 35].

**Acknowledgments:** N. Zander and Z. Yosibash gratefully acknowledge the financial support of the German Research Foundation (DFG) under grant RA 624/19-1. The authors also like to thank D. Schillinger for fruitful discussions on the topics addressed in this paper. The authors also thank A. Düster for his valuable input.

- [1] A. Abedian, J. Parvizian, A. Düster, H. Khademyzadeh, and E. Rank. Performance of different integration schemes in facing discontinuities in the Finite Cell Method. *International Journal of Computational Methods*, submitted, 2011.
- [2] D. N. Arnold, F. Brezzi, B. Cockburn, and L. D. Marini. Unified Analysis of Discontinuous Galerkin Methods for Elliptic Problems. *SIAM Journal on Numerical Analysis*, 39(5):1749, 2002. doi: 10.1137/S0036142901384162.
- [3] Y. Bazilevs and T. Hughes. Weak imposition of Dirichlet boundary conditions in fluid mechanics. *Computers & Fluids*, 36(1):12–26, 2007. doi: 10.1016/j.compfluid.2005.07.012.
- [4] T. Belytschko, T. Black, Y. Y. Lu, and L. Gu. Element-free galerkin methods. *International Journal for Numerical Methods in Engineering*, 37:229–256, 1994.
- [5] S. Bindick, M. Stiebler, and M. Krafczyk. Fast kd-tree based hierarchical radiosity for radiative heat transport problems. *International Journal for Numerical Methods in Engineering*, 86:1082–1100, 2011.
- [6] Q. Cai, S. Kollmannsberger, R. Mundani, and E. Rank. The finite cell method for spatially varying dispersions in coupled multispecies reactive transport problems. In *Proceedings of the International Conference on*

*Computational Methods for Coupled Problems in Science and Engineering*, Kos Island, Greece, 2011.

- [7] Q. Cai, S. Kollmannsberger, R. Mundani, and E. Rank. The finite cell method for solute transport problems in porous media. In *Proceedings of the International Conference on Finite Elements in Flow Problems*, Garching, Germany, 2011.
- [8] Q. Cai, S. Kollmannsberger, and E. Rank. The Finite Cell Method for Convection-Diffusion Problems in Porous Media. *International Journal for Numerical Methods in Engineering*, submitted, 2011.
- [9] K. Cheng and T.-P. Fries. Higher-order XFEM for curved strong and weak discontinuities. *International Journal for Numerical Methods in Engineering*, 82:564–590, 2009.
- [10] K. Dréau, N. Chevaugeon, and N. Moës. Studied X-FEM enrichment to handle material interfaces with higher order finite element. *Computer Methods in Applied Mechanics and Engineering*, 199(29-32):1922 – 1936, 2010.
- [11] A. Düster, J. Parvizian, Z. Yang, and E. Rank. The finite cell method for three-dimensional problems of solid mechanics. *Computer Methods in Applied Mechanics and Engineering*, 197:3768–3782, 2008.
- [12] A. Düster, J. Parvizian, and E. Rank. Topology optimization based on the finite cell method. *Proceedings in Applied Mathematics and Mechanics*, 10:151–152, 2010.
- [13] A. Embar, J. Dolbow, and I. Harari. Imposing Dirichlet boundary conditions with Nitsche’s method and spline-based finite elements. *International Journal for Numerical Methods in Engineering*, 83(7):877–898, 2010.
- [14] C. A. Felippa. Fluid-Structure Interaction lecture notes. <http://www.colorado.edu/engineering/CAS/courses.d/FSI.d/>, 2004.
- [15] S. Fernández-Méndez and A. Huerta. Imposing essential boundary conditions in mesh-free methods. *Computer Methods in Applied Mechanics and Engineering*, 193(12-14):1257 – 1275, 2004.

- [16] T.-P. Fries and T. Belytschko. The extended/generalized finite element method: An overview of the method and its applications. *International Journal for Numerical Methods in Engineering*, 84(3):253–304, 2010.
- [17] A. Gerstenberger and W. Wall. An eXtended Finite Element Method / Lagrange Multiplier based approach for fluid-structure interaction. *Computer Methods in Applied Mechanics and Engineering*, 197:1699–1714, 2008.
- [18] A. Gerstenberger and W. Wall. An embedded Dirichlet formulation for 3D continua. *International Journal for Numerical Methods in Engineering*, 82:537–563, 2010.
- [19] R. Glowinski and Y. Kuznetsov. Distributed Lagrange multipliers based on fictitious domain method for second order elliptic problems. *Computer Methods in Applied Mechanics and Engineering*, 196:1498–1506, 2007.
- [20] T. J. R. Hughes. *The Finite Element Method: Linear Static and Dynamic Finite Element Analysis*. Dover Publications, 2000. ISBN 0-486-41181-8.
- [21] R. Löhner, J. Cebral, F. Camelli, J. Baum, E. Mestreau, and O. Soto. Adaptive embedded/immersed unstructured grid techniques. *Archives Of Computational Methods In Engineering*, 14:279–301, 2007.
- [22] R. Mittal and G. Iaccarino. Immersed Boundary Method. *Annual Review Fluid Mechanics*, 37:239–260, 2005.
- [23] M. Mounnassi, J. Belouettar, E. Béchet, S. Bordas, Q. D., and M. Potier-Ferry. Finite element analysis on implicitly defined domains: An accurate representation based on arbitrary parametric surfaces. *Computer Methods in Applied Mechanics and Engineering*, 200:774–796, 2011.
- [24] J. Nitsche. Über ein variationsprinzip zur Lösung von Dirichlet-Problemen bei Verwendung von Teilräumen, die keinen Randbedingungen unterworfen sind. *Abhandlungen aus dem Mathematischen Seminar der Universität Hamburg*, 36(1):9–15, 1971.

- [25] H. Parkus. *Thermoelasticity*. Springer, Wien, New York, 2. edition, 1968. ISBN 3-211-81375-6.
- [26] J. Parvizian, A. Düster, and E. Rank. Finite cell method – h- and p-extension for embedded domain problems in solid mechanics. *Computational Mechanics*, 41:121–133, 2007.
- [27] C. Peskin. The Immersed Boundary Method. *Acta Numerica*, 11:1–39, 2002.
- [28] W. Press, S. Teukolsky, W. Vetterling, and B. Flannery. *Numerical Recipes in C++. The Art of Scientific Computing*. Cambridge University Press, 2. edition, 2002. ISBN 0-521-75033-4.
- [29] M. Ruess, R.-P. Mundani, A. Düster, E. Rank, R. Burgkart, R. Gradinger, and R. Westermann. Computational Steering for Orthopaedics. *Bio Materialien*, 9 (1/2):53, 2008.
- [30] M. Ruess, Z. Yosibash, and E. Rank. Application of the Finite Cell Method to patient-specific femur simulations. *Proceedings in Applied Mathematics and Mechanics*, 2011.
- [31] M. Ruess, D. Tal, N. Trabelsi, Z. Yosibash, and E. Rank. The finite cell method for bone simulations: Verification and validation. *Biomechanics and Modeling in Mechanobiology*, 11(3):425–437, 2012.
- [32] M. H. Sadd. *Elasticity - Theory, Applications, and Numerics (2nd Edition)*. Elsevier, 2009.
- [33] D. Schillinger and E. Rank. An unfitted hp-adaptive finite element method based on hierarchical B-splines for interface problems of complex geometry. *Computer Methods in Applied Mechanics and Engineering*, 200(47 - 48):3358 – 3380, 2011. doi: 10.1016/j.cma.2011.08.002.
- [34] D. Schillinger, L. Dedè, M. A. Scott, J. A. Evans, M. J. Borden, E. Rank, and T. J. Hughes. An isogeometric design-through-analysis methodology based on adaptive hierarchical refinement of NURBS, immersed boundary methods, and T-spline CAD surfaces. *Computer Methods in Applied Mechanics and Engineering*, in press, 2012. doi: 10.1016/j.cma.2012.03.017.

- [35] D. Schillinger, A. Düster, and E. Rank. The hp-d-adaptive finite cell method for geometrically nonlinear problems of solid mechanics. *International Journal for Numerical Methods in Engineering*, 89(9):1171–1202, 2012. doi: 10.1002/nme.3289.
- [36] D. Schillinger, M. Ruess, N. Zander, Y. Bazilevs, A. Düster, and E. Rank. Small and large deformation analysis with the p- and B-spline versions of the Finite Cell Method. *Computational Mechanics*, 2012. doi: 10.1007/s00466-012-0684-z.
- [37] B. Szabó and I. Babuška. *Finite element analysis*. John Wiley & Sons, 1991. ISBN 0-471-50273-1.
- [38] B. Szabó, A. Düster, and E. Rank. The p-version of the Finite Element Method. In E. Stein, R. de Borst, and T. J. R. Hughes, editors, *Encyclopedia of Computational Mechanics*, volume 1, chapter 5, pages 119–139. John Wiley & Sons, 2004.
- [39] P. Vos, R. Loon, and S. Sherwin. A comparison of fictitious domain methods appropriate for spectral/hp element discretizations. *Computer Methods in Applied Mechanics and Engineering*, 197:2275–2289, 2008.
- [40] Z. Yang, M. Ruess, S. Kollmannsberger, A. Düster, and E. Rank. An efficient integration technique for the voxel-based Finite Cell Method. *International Journal for Numerical Methods in Engineering*, Accepted for publication, 2011.
- [41] Z. Yang, S. Kollmannsberger, A. Düster, M. Ruess, R. Burgkart, E. Garcia, and E. Rank. Non-standard bone simulation: Interactive numerical analysis by computational steering. *Computing and Visualization in Science*, 14(5):207–216, 2012.
- [42] N. Zander. The Finite Cell Method for Linear Thermoelasticity. Master’s thesis, Technische Universität München, 2011.
- [43] X. Zhuang. *Meshless methods: theory and application in 3D fracture modelling with level sets*. PhD thesis, University of Durham, 2010.
- [44] O. Zienkiewicz and R. Taylor. *The Finite Element Method – Its Basis and Fundamentals*, volume 1. Butterworth-Heinemann, 6th edition, 2005. ISBN 0-7506-6320-0.